ACS Photonics

Article

pubs.acs.org/journal/apchd5

Light Management in Upconverting Nanoparticles: Ultrasmall Core/Shell Architectures to Tune the Emission Color

Marta Quintanilla,† Fuqiang Ren,† Dongling Ma,* and Fiorenzo Vetrone*

Institut National de la Recherche Scientifique - Énergie, Matériaux et Télécommunications, Université du Québec, 1650 Boulevard Lionel-Boulet, Varennes, Quebec J3X 1S2, Canada

Supporting Information

ABSTRACT: Ultrasmall $NaGdF_4$ nanoparticles with core/shell and core/shell/shell architectures have been synthesized following a microwave-based thermolysis procedure, allowing us to rapidly obtain homogeneous nanoparticles compared to conventional heating. To analyze the possibilities of the proposed structure in terms of tuning the emission color, core and shells have been doped with different lanthanide ion pairs (either Er^{3+}/Yb^{3+} and/or Tm^{3+}/Yb^{3+}), keeping them therefore spatially separated inside the different layers of the nanoparticles. Here, we demonstrate that the position of the dopants inside the nanoparticles affects the intensity of the different emission bands of the luminescing Tm^{3+} and Er^{3+} ions and show how it has a relevant effect on the overall emission color of the luminescence obtained after 975 nm excitation.

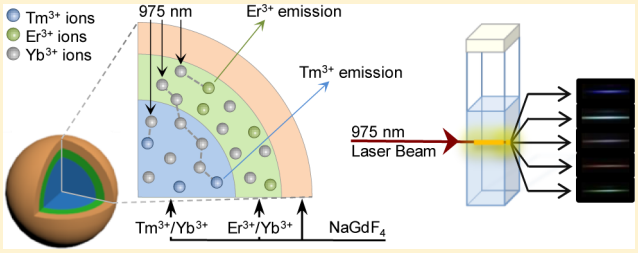

KEYWORDS: *upconverting nanoparticles, microwave synthesis, core/shell, color tuning, energy migration, lanthanides*

Since the last century, nanosized particles have elicited a great deal of excitement with the promise to bring forth a paradigm shift by provoking a technological (and biotechnological) transformation. In the vanguard of this push toward the nanoscale, luminescent nanoparticles have graduated from mere academic curiosity to being seriously considered for use in a plethora of applications.[1−3] Perhaps their biggest impact will come in their use in biology, where their nanometric dimensions, similar to many biological structures, can potentially lead to their use in diverse applications such as optical probes for sensing, diagnosis, and even therapeutics for a slate of diseases.[3−7] In many cases, this new generation of luminescent nanoparticles forms the nuclei of multifunctional nanoplatforms where two or more of the functions described above can be carried out (either sequentially or simultaneously) in one nanoscale platform.[8,9]

Traditionally, many of these luminescent nanoparticles studied have been optically excited following a conventional route whereby ultraviolet (UV) or visible light emissions are observed following excitation with higher energy photons. This can lead to various complications since often biological samples have inherent chromophores or fluorophores that could emit light when excited with high-energy radiation.[10,11] Consequently, their presence generates a large background autofluorescence that complicates the detection of the emission from the nanoparticles unless more complex optical techniques are employed. Moreover, exciting with UV photons hinders the tissue penetration capabilities and can also irreversibly cause photodamage to the specimen under study, potentially limiting the scope of their possible applications.

Excitation with near-infrared (NIR) light could alleviate some of the problems associated with conventional high-energy light excitation, especially considering that biological tissues have an optical transparency window in the NIR region (approximately 700−1000 nm).[12] Therefore, the possibility of using long-wavelength (or low-energy) NIR light as an excitation source to generate shorter wavelength photons (in either the UV, visible, or even NIR ranges) is remarkably attractive for biological applications.[1,2,4,13,14] For example, it becomes possible to use NIR light to trigger further photoactivated processes whereby currently only UV or blue light can be used, as is the case in photocatalysis, photothermal/photodynamic therapies, or drug delivery.[1,15]

In this context, several materials have been proposed as nanoemitters using a NIR excitation strategy. Metal nanoparticles or semiconductor quantum dots are among the most explored materials for these applications.[16,17] However, to obtain visible emissions following NIR illumination requires, in this case, ultrafast excitation. This is due to the absence of available intermediate energy states, which implies that population of the excited state requires the simultaneous absorption of more than one photon.[18] This is, from the point of view of the applications, a clear economical drawback, as these excitation sources can be very costly. Bearing in mind these facts, a different family of nanoparticles based on lanthanide-doped materials is currently being considered. In this case, a transparent nanocrystal, most commonly fluoride-based, is doped with a certain concentration of lanthanide ions.

Received: February 25, 2014
Published: July 7, 2014

Due to the 4f electronic configuration of the lanthanides, with the valence electrons shielded by the filled outer 5s, 6s, and 5p shells, they add to the host matrix a series of available excited states at well-known fixed energies weakly dependent on the environment. These states can be used to promote electrons, in a ladder-like process, thereby making it possible to obtain higher energy emissions (in the UV, visible, or even NIR) following NIR excitation.[19,20] Moreover, since the intermediate energy states used for this process, known as upconversion, are not only real states but also characteristic for their relatively long lifetimes, the higher energy emissions can be obtained from NIR excitation using inexpensive continuous wave diode lasers as the excitation source. This is in stark contrast, as mentioned, to the case of semiconductor or metal nanoparticles.

In the case of quantum dots and metal nanorods, the wavelength of the emission can be modified by changing the size or aspect ratio of the nanostructures, respectively. Conversely, for lanthanide-doped nanoparticles, size and shape have an effect on the intensity of the light emissions, but not on the obtained wavelengths. Instead, the "color" of the emission can be tuned by altering the specific lanthanide ions used as dopants or their concentrations. For instance, Er^{3+} ions are characteristic for their green and red emissions, while Tm^{3+} ions generally emit in the NIR, blue, and ultraviolet range of the spectrum. In both cases, the upconversion process can be sensitized with Yb^{3+} ions, since the transitions associated with their single excited state allow for the absorption and emission of NIR photons (at ca. 975 nm). Additionally, Yb^{3+} ions have a higher absorption cross section than Er^{3+} or Tm^{3+} at that wavelength and are able to efficiently transfer energy to both Er^{3+} and Tm^{3+} ions, thus triggering the upconversion processes that will generate higher energy light.[21]

Taking these into account, it would be possible to use one single NIR excitation source (at 975 nm) to excite a single nanoparticle doped with Yb^{3+}, Er^{3+}, and Tm^{3+} ions in order to obtain red (R), green (G), and blue (B) emissions. This lays the foundation for the development of a versatile RGB-based nanosystem that can provide a wide range of emission colors.[22] Unfortunately, managing the color of the resulting emission light is not a simple feat due to the multitude of energy transfer processes that can occur between lanthanide ions, which are strongly dependent on the distance separating the dopant ions and, thus, are strongly affected by the dopant concentration. For instance, in a tridoped nanoparticle ($Yb^{3+}/Er^{3+}/Tm^{3+}$) the three needed emission colors, blue green, and red, would be present, but the relative intensities of the emissions would be difficult to control in order to tune the emission, since it will be strongly affected by the energy transfer processes from Er^{3+} to Er^{3+} and/or from Tm^{3+} to Tm^{3+} as well as the concomitant energy transfer processes between Er^{3+} and Tm^{3+} ions that will quench certain emissions and enhance others, generally reducing the range of emission colors that can be obtained for lanthanide-doped nanoparticles.[23−26]

In this work, we develop a lanthanide-doped upconverting $NaGdF_4$ nanoparticle possessing a core/shell architecture with different dopants in the core and the shell. The goal is to spatially separate the Er^{3+} and Tm^{3+} ions in order to reduce the transfer of energy between them. Furthermore, the nanoparticles are prepared using a modified thermal decomposition process that employs microwave-assisted heating rather than conventional heating. The use of microwave reactors is a very recent innovation for the synthesis of upconverting nanoparticles that yields the possibility of obtaining highly homogeneous particles, from both the morphological and structural point of view, and in a very short time frame.[27−31] Until recently, microwave-assisted synthesis has successfully demonstrated the possibility of obtaining ultrasmall lanthanide-doped nanoparticles, but the synthesis of more complicated structures including core/shell nanoarchitectures has been a challenge. Here, we synthesize multilayered nanostructures such as core/shell and core/shell/shell while investigating the ability to control the light output of the nanoparticles by segregating the luminescent lanthanide ions in individual portions of the nanoparticle.

With this ultimate goal, we performed a sequential process of up to three treatment steps in a microwave autoclave. The synthesis procedure for the lanthanide-doped nanoparticles was based on the thermal decomposition technique using metal trifluoroacetates as precursors[32] that were dispersed in a 0.5:0.5:1 solution of oleic acid, oleylamine, and 1-octadecene (refer to the Supporting Information for further details about the synthesis procedure). The selected concentrations of dopants are, in the first approach, $[Tm^{3+}]$ = 0.2 mol %/$[Yb^{3+}]$ = 20 mol % and $[Er^{3+}]$ = 2 mol %/$[Yb^{3+}]$ = 20 mol %, since these values are in the range that have been demonstrated to be optimum to get intense blue emissions from Tm^{3+} ions as well as green and red emissions from Er^{3+} ions, respectively.[33−35]

The initial microwave-assisted synthesis of ultrasmall $NaGdF_4$:Tm^{3+}, Yb^{3+} nanoparticles took place in a tightly closed vessel for 10 min at 300 °C and yielded spherical and highly homogeneous nanoparticles with a size of 6.1 ± 0.8 nm (Figure 1A). Moreover, the XRD measurements, also shown in Figure 1, clearly showed that the nanoparticles crystallized in the α-phase (cubic phase) of $NaGdF_4$. Subsequently, we added to the vessel containing the core-only $NaGdF_4$:Tm^{3+}, Yb^{3+} nanoparticles the necessary precursors to grow an active (i.e., luminescent) shell of $NaGdF_4$:Er^{3+}, Yb^{3+} and treated the mixture in the microwave for 10 min at 270 °C. Further TEM analysis (Figure 1B) demonstrated that the new nanoparticles kept the same spherical shape and crystal phase as the parent core-only nanoparticles. However, as expected, their average size was observed to be larger than in the previous case (7.5 ± 0.5 nm).

It is well known that growing an undoped (passive) shell around upconverting nanoparticles would increase the intensity of the upconverted luminescence because it isolates the active ions (sensitizers and activators) from the environment.[36−38] Moreover, since the effect of the environment will not necessarily affect every dopant ion equally, it will also change the overall upconverted emission color. Aiming to analyze this effect, as a final step, we grew a third undoped layer of $NaGdF_4$ on the already synthesized core/shell nanoparticles by means of a third microwave step equivalent to the previous one, this time for 1 min at 270 °C. The resulting nanoparticles are shown in Figure 1C. The final core/shell/shell upconverting nanoparticles still show a homogeneous spherical morphology and α crystal phase, but they possess an even larger size than previous (8.5 ± 0.8 nm). High-resolution TEM was performed on these final core/shell/shell nanoparticles (Figure 1D) and nicely demonstrated that the particles were monocrystalline, with clearly visible lattice fringes and did not show any interphases.

To get a clearer idea of the size evolution of the nanoparticles after all the subsequent synthesis steps, the particle size

dx.doi.org/10.1021/ph500208q | ACS Photonics 2014, 1, 662−669

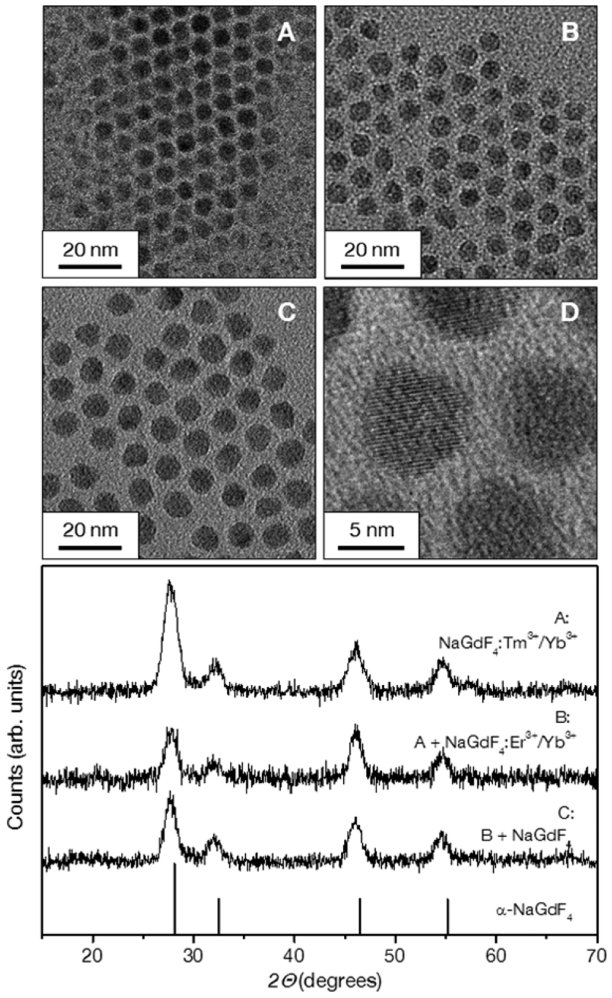

Figure 1. TEM micrographs of the nanoparticles obtained with $NaGdF_4:Tm^{3+}$, Yb^{3+} precursors (A), core/shell nanoparticles obtained from A adding $NaGdF_4:Er^{3+}$, Yb^{3+} precursors (B), and the core/shell/shell nanoparticles obtained after the growth of an undoped $NaGdF_4$ shell over B (C). A higher magnification of these core/shell/shell particles is shown in D. Below, the XRD patterns of each sample compared to the pattern for α-$NaGdF_4$ (JCPDS 00-027-0697) are shown.

distributions obtained after measuring several hundreds of particles from the TEM images are plotted in Figure 2. As it can be seen, in every case, single distributions are obtained, clearly demonstrating the homogeneity of the nanoparticles. This result supports the notion that after each successive growth process one single type of nanoparticle is synthesized, since particle size distributions with two (or three) peaks would likely be obtained if the subsequent addition of precursors were creating new nuclei instead of growing a shell on the previous particles.

From Figure 2 it is also clear that the nanoparticles become larger after each growth step, initially starting from approximately 6 nm after the growth of the core-only nanoparticles to a final size of 8.5 nm for the core/shell/shell nanoparticles after the addition of two more sets of precursors. Thus, this size increase is also consistent with our hypothesis that the ultrasmall nanoparticles synthesized at the onset become the core in a core/shell structure after the second step, and these core/shell nanoparticles become the core/shell/shell structures after another addition of precursors.

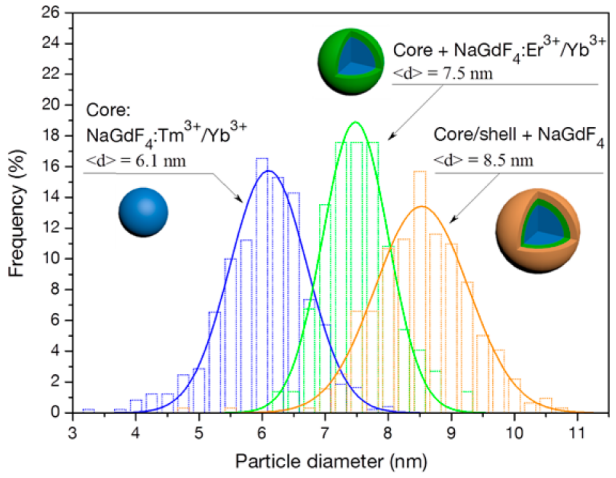

Figure 2. Size distribution of the upconverting nanoparticles obtained after each synthesis step. First $NaGdF_4:Tm^{3+}$, Yb^{3+} core, then $NaGdF_4:Tm^{3+}$, Yb^{3+} core with $NaGdF_4:Er^{3+}$, Yb^{3+} shell, and finally $NaGdF_4:Tm^{3+}$, Yb^{3+} with two shells, $NaGdF_4:Er^{3+}$, Yb^{3+} (inner shell) and undoped $NaGdF_4$ (outermost shell).

To underscore the reproducibility of these results, the syntheses were repeated up to four times following the same protocol and using the same concentrations of dopants. In this way, average values of the nanoparticle diameters of 6.0 ± 0.2 nm for the core-only nanoparticles, 7.9 ± 0.4 nm for the core/shell nanoparticles, and 8.9 ± 0.4 nm for the core/shell/shell nanoparticles were calculated. The errors in these values represent the standard deviation obtained for the average of the four averaged sizes, and they show that the size of the nanoparticles is, to a large extent, the same in every synthesis.

As a further test, it was considered that since the nanoparticles were not washed between steps, the possibility still persisted that any unreacted precursors remaining in the solvent could account for the growth of new nanoparticles. To test this hypothesis, some of the nanoparticles shown in Figure 1B (core/shell nanoparticles before washing) were heat treated in the microwave for 10 min at 270 °C, under the same conditions that were used to obtain the nanoparticles in Figure 1C (core/shell/shell), but without additional precursors. In this experiment (Figure S1) a difference of 0.2 nm in the average size of the nanoparticles was found, a value that is within the experimental error and much smaller than the observed size increase of the nanoparticles when precursors are added to the solution. Therefore, we can conclude that our observed size increase was undoubtedly due to the new precursors added.

To further demonstrate that the new nanostructure we synthesized in fact had a core/shell/shell architecture, we studied the upconversion luminescence properties of the nanoparticles at each successive step of the synthesis. Figure 3A shows the upconverted emission spectrum of each sample after excitation at 975 nm (excitation power density on the focus 2 W/mm^2). The electronic 4f transitions responsible for each emission are labeled in the figure and are schematically shown in Figure 4, for both the Tm^{3+} and Er^{3+} emission bands. According to the generally accepted mechanisms for upconversion in Tm^{3+}/Yb^{3+} and Er^{3+}/Yb^{3+} systems,[21,39,40] the laser excitation at 975 nm is mainly absorbed by Yb^{3+} ions and then transferred to the co-dopant luminescing ion (Tm^{3+} or Er^{3+}), which is playing the role of acceptor in the energy transfer process. Then, in a second step, another Yb^{3+} ion

dx.doi.org/10.1021/ph500208q | ACS Photonics 2014, 1, 662−669

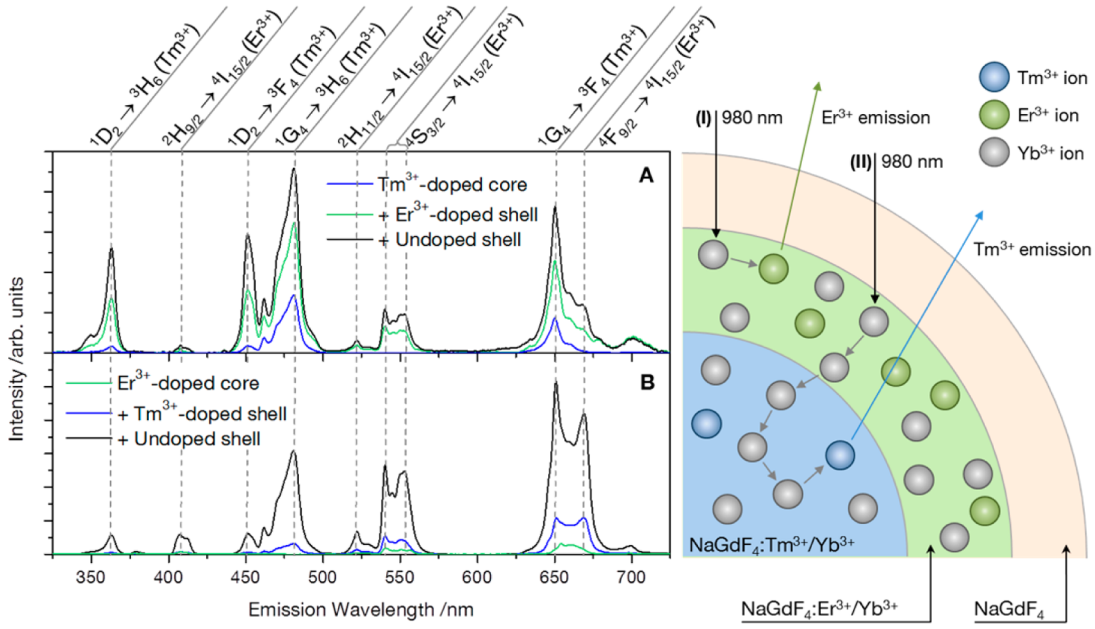

Figure 3. (A) Upconversion emission spectra obtained after 975 nm excitation for $NaGdF_4$:Tm^{3+}, Yb^{3+} core-only nanoparticles (blue line) and the successive core/shell (green line) and core/shell/shell (black line) structures with $NaGdF_4$:Er^{3+}, Yb^{3+} in the first shell and undoped $NaGdF_4$ in the second shell. (B) Upconversion emission spectra obtained for $NaGdF_4$:Er^{3+}, Yb^{3+} (blue line), core/shell (green line), and core/shell/shell (black line) nanoparticles with $NaGdF_4$:Tm^{3+}, Yb^{3+} in the first shell and undoped $NaGdF_4$ in the second shell. In every case, the nanoparticle concentration is 1 wt % in hexane. On the right side a scheme has been added of a core/shell/shell nanoparticle showing the migration mechanism between Yb^{3+} ions and how it can affect the emission of the different layers.

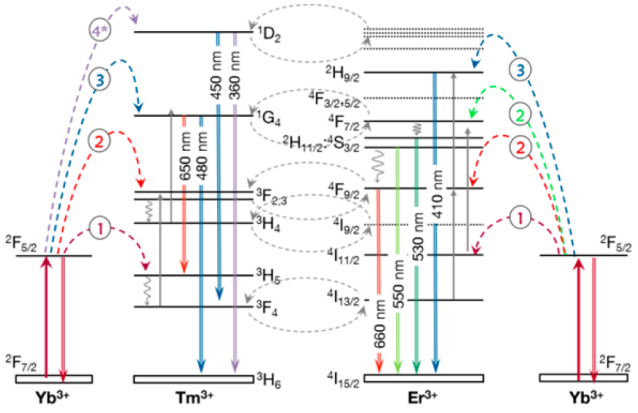

Figure 4. Energy level diagrams of Yb^{3+}, Tm^{3+}, and Er^{3+} dopant ions. The mechanisms of upconversion (dashed colored arrows), the possible Er^{3+}–Tm^{3+} energy transfer processes (dashed gray arrows), and the electronic transitions responsible for the observed emissions (solid arrows) are depicted.

previously excited can transfer its energy to the co-dopant that was excited to the intermediate excited state in the previous step. This process can be repeated several times as long as there is an acceptor ion close enough to the excited Yb^{3+} ions able to accept its energy. In this way, according to the diagram in Figure 4, it is possible to excite the blue-emitting levels of Tm^{3+} in three energy transfer steps (i.e., a three-photon process), while the green- and red-emitting levels of Er^{3+} can be excited in two steps (two-photon process). According to Figure 3, also a violet emission band is observed at ca. 360 nm associated with the $^1D_2$ state of the Tm^{3+} ions. The population path of this level involves two different mechanisms that occur concomitantly: a fourth energy transfer from Yb^{3+} ions (labeled with an asterisk in Figure 4) and Tm^{3+} to Tm^{3+} energy transfer mechanisms (shown in the Supporting Information Figure S2).[41,42]

It is clear from Figure 3A that the core-only nanoparticles obtained in one single microwave step, where only $NaGdF_4$:Tm^{3+}, Yb^{3+} precursors are used, show the characteristic upconverted emissions of Tm^{3+} ions with bands in the violet (around 360 nm, corresponding to $^1D_2 \rightarrow {}^3H_6$ transition), blue (two bands around 450 and 470 nm, corresponding to $^1D_2 \rightarrow {}^3F_4$ and $^1G_4 \rightarrow {}^3H_6$ transitions, respectively), and red (around 650 nm, $^1G_4 \rightarrow {}^3F_4$ transition) ranges. After the growth of the first shell, this time using $NaGdF_4$:Er^{3+}, Yb^{3+} precursors, three new emission bands associated with Er^{3+} ions are observed in the emission spectrum: one in the red (at around 670 nm, $^4F_{9/2} \rightarrow {}^4I_{15/2}$ transition) and two more in the green range (at around 520 and 550 nm, $^2H_{11/2} \rightarrow {}^4I_{15/2}$ and $^4S_{3/2} \rightarrow {}^4I_{15/2}$ transitions, respectively).

Nevertheless, this is not the only observed effect of the Er^{3+}/Yb^{3+}-doped shell. Also, according to Figure 3A, the growth of this shell has triggered a general enhancement of the Tm^{3+} emission intensities from the Tm^{3+}/Yb^{3+}-doped core. This effect can be explained considering that the high-energy vibrational modes of the adsorbed species on the surface of the nanoparticles including the oleic acid and oleylamine capping ligands are known to induce quenching of the luminescence of lanthanide ions.[43,44] To avoid this reduction in the luminescence intensity, a common option is to passivate the surface of the nanoparticles by growing a protecting shell of undoped host material.[36,38,45,46] In the present situation, the active Er^{3+}/Yb^{3+}-doped shell grown around the Tm^{3+}/Yb^{3+}-doped core can have this effect and, thus, trigger the enhancement observed in Figure 3A. Since this enhancement is linked to a core/shell nanoarchitecture, its presence can be

dx.doi.org/10.1021/ph500208q | ACS Photonics 2014, 1, 662–669

considered as additional proof of the success in growing this kind of structure.

It stands to reason that if a third shell were grown around the $NaGdF_4$:Tm^{3+}, Yb^{3+} core/$NaGdF_4$:Er^{3+}, Yb^{3+} shell nanoparticles, this time undoped $NaGdF_4$, the same enhancement effect should be observed for the luminescence attributed to the Er^{3+}/Yb^{3+}-doped shell. It can be seen from Figure 3 that there is a definite enhancement of the luminescence; however, it is observed for both the Tm^{3+} ions in the core and the Er^{3+} ions in the intermediate shell. The fact that the core is still affected by this outer third shell, despite the existence of the intermediate second shell layer, can be related to the presence of sensitizer Yb^{3+} ions both in the core and in the intermediate shell (see scheme on the right side of Figure 3). Since the Yb^{3+} concentration is relatively high (20 mol %) in both areas, energy transfer processes between Yb^{3+} ions, i.e., energy migration, become probable and can offer a path for the absorbed energy to travel between the core and the intermediate shell. Gd^{3+} ions have also been previously demonstrated to account for interlayer energy migration.[47] In our case, though, light emission from Gd^{3+} ions is not detected, and thus their contribution should be smaller since their excited state is not expected to be highly populated. Therefore, due to energy migration through either Yb^{3+} or Gd^{3+} ions, minimizing the quenching sites on the surface of the intermediate shell can have a positive effect not only on the luminescence of this shell but also on the luminescence of the core.

Due to the different quenching levels and energy transfer/migration processes in each of the nanoparticle layers, the upconverted luminescence spectrum of the core/shell nanoparticle (and further the core/shell/shell structure) with Tm^{3+}/Yb^{3+} ions in the core and Er^{3+}/Yb^{3+} ions in the shell is not expected to be identical to the upconverted luminescence of the core/shell structure in which the core and shell dopants are inverted (i.e., Er^{3+}/Yb^{3+} ions in the core and Tm^{3+}/Yb^{3+} ions in the shell). Moreover, since the upconversion mechanism that populates the blue-emitting levels of the Tm^{3+} ions involves a three-step process, its dependence on any modification of the excitation or the donor ions will generally be stronger than in the case of the two-step upconversion process associated with Er^{3+} ions. Following this idea, core/shell/shell nanoparticles were synthesized where the location of the luminescent ion pairs were swapped, i.e., with Er^{3+}/Yb^{3+} dopants in the core and Tm^{3+}/Yb^{3+} dopants in the shell. The size and morphologic properties of these new nanoparticles were nearly identical to the ones previously discussed (see Figures S3 and S4). Interestingly though, the upconverted luminescence spectra of the nanoparticles were different. It is clear from the emission curves shown in Figure 3B that the intensity ratios between the different bands, attributed to the Er^{3+} and Tm^{3+} ions in the luminescence spectrum, have changed compared to the nanoparticles that have Tm^{3+}/Yb^{3+} ions in the core. Once again, the fact that the luminescence spectra of the Er^{3+}-core/Tm^{3+}-shell and Tm^{3+}-core/Er^{3+}-shell nanoparticles are different confirms our hypothesis that core/shell nanostructures were obtained, while eliminating the possibility that two types of nanoparticles with different dopants were synthesized (i.e., individual $NaGdF_4$:Er^{3+}, Yb^{3+} and $NaGdF_4$:Tm^{3+}, Yb^{3+} nanoparticles). There are inherent difficulties in demonstrating the existence of a core/shell system where both the core and the shell are composed of the same material, especially in the case of lanthanide-doped nanoparticles. In some cases, it can require elaborate instrumentation, which may not be routinely available. To demonstrate this, Abel et al.[48] used X-ray photoelectron spectroscopy with a tunable synchrotron radiation source. While this method provides incontrovertible proof, access to such equipment may be an issue for some. In contrast, the optical method described here, which relies on inverting the dopant ions in the core and shell, presents a straightforward and facile method for ascertaining that a core/shell system is in fact present. Furthermore, this method is not limited to upconverting nanoparticles and is easily applicable to other lanthanide-doped systems as long as the co-dopants present different luminescence spectra.

The aforementioned changes in the intensity ratios between the emission bands associated with the Er^{3+} or Tm^{3+} transitions in the blue, green, and red regions account for strong differences in the color of the overall emission, i.e., the color of the emitted light that can be seen with the naked eye (Figure 5). To demonstrate these changes, the CIE color coordinates

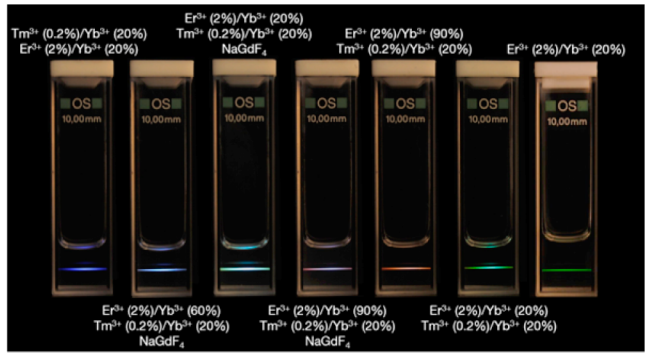

Figure 5. Digital images of 1 wt % solutions of upconverting nanoparticles in hexane using an excitation laser source at 975 nm. The pictures have been taken with a Nikon camera (2 s exposure time).

associated with each spectrum in Figure 3 have been calculated and are depicted in the diagram shown in Figure 6. It is clear from the figure that the Er^{3+}/Yb^{3+} core-only nanoparticles show a green emission color, while the Tm^{3+}/Yb^{3+} core-only nanoparticles are associated with a blue emission color. Then, when both ion pairs are incorporated in the same nanoparticle structure albeit spatially separated, different possibilities between these two extremes can be obtained depending on the location of each ion inside the nanoparticle. Moreover, it is also clear that the outer shell in the core/shell/shell architecture, although it is undoped, helps to change the emission color.

As it has been shown, using this strategy, it is possible to tune the emission color of the upconverting nanoparticles using a single excitation wavelength. Up to that point, though, the range of available colors is restricted to the line shown in Figure 6 between the pure Er^{3+}/Yb^{3+} and Tm^{3+}/Yb^{3+}-doped core-only nanoparticles ([Yb^{3+}] = 20 mol %, [Tm^{3+}] = 0.2 mol %, and [Er^{3+}] = 2 mol %). Nevertheless, different strategies can be applied to broaden the range of color tuning. For instance, the intensity of the emissions and the intensity ratios between the different emissions will change with doping concentration, changing thus the overall emission color. In the case of Tm^{3+} ions different shades between blue and magenta can be obtained modifying either the Tm^{3+} or Yb^{3+} concentrations.[33] In the same way, in the Yb^{3+}/Er^{3+} area of the nanoparticles,

dx.doi.org/10.1021/ph500208q | ACS Photonics 2014, 1, 662−669

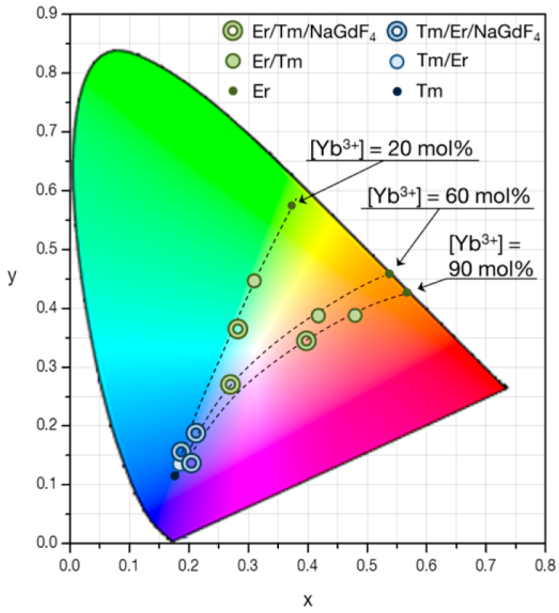

Figure 6. CIE color coordinates obtained from the recorded spectra for $NaGdF_4$:Tm^{3+}, Yb^{3+} and $NaGdF_4$:Er^{3+}, Yb^{3+} core-only nanoparticles, and the core/shell and the core/shell/shell structures obtained. For the sake of clarity, the data with the same Yb^{3+} concentration are linked with dashed black lines.

higher Yb^{3+} contents strongly increase the red emissions coming from Er^{3+} ions compared to the green ones.[35]

Thanks to the fact that both pairs of ions are spatially separated in the nanoparticles, these two mentioned dependencies are expected to still work in our case. Otherwise, if Er^{3+} and Tm^{3+} ions were doped together in the same host material, they would efficiently transfer energy between themselves. As an example, in Figure 4 some of the possible resonant energy transfer processes between them are marked with gray dashed arrows. These energy transfers between Er^{3+} and Tm^{3+} have been extensively studied in several hosts, both experimentally and theoretically, and it has been demonstrated that the option with a higher probability takes place between the lowest excited-state levels ($^4I_{13/2} \rightarrow {}^4I_{15/2}$ (Er^{3+}): $^3H_6 \rightarrow {}^3F_4$ (Tm^{3+})) and accounts for the depopulation of Er^{3+} ions to populate Tm^{3+} ions.[23−26] Such a modification in these low-energy states, which are at the root of every upconversion process, results in an intensification of the emissions from Tm^{3+} ions to the detriment of Er^{3+} ones. This, in terms of emission "color", means that blue light is generally obtained, or depending on the concentration of dopants and on the presence of Yb^{3+} ions, white light is also achievable.[35,49−53] Nevertheless, as a further test, particles with the three dopants mixed together have been synthesized and are discussed in the Supporting Information (Figure S5).

In this work, to further explore the possibilities that the core/shell or core/shell/shell nanostructures offer in terms of emission color management, the selected strategy has been to change the Yb^{3+} concentration in the Yb^{3+}/Er^{3+} area of the particles. Thus, samples with different Yb^{3+}/Er^{3+} content have been prepared (Yb^{3+}/Er^{3+} = 20 mol %/2 mol %; 60 mol %/2 mol %; 90 mol %/2 mol %), while Yb^{3+}/Tm^{3+} concentration has been kept constant (Yb^{3+}/Tm^{3+} = 20 mol %/0.2 mol %). The CIE coordinates calculated from the emission spectra of the two new families of nanoparticles are shown in Figure 6 (the upconverted emission spectra can be seen in Figure S7).

Also, to offer a visual example of the obtained results, in Figure 5 a digital photograph of some of the samples excited with 975 nm light is shown. It should be noted that we performed an XRD analysis of the sample heavily doped with Yb^{3+} to determine if any changes in the crystalline structure were present, which could affect the luminescence (see Figure S6). Both samples show equivalent patterns, indicating that they both crystallized in the cubic phase. Nevertheless, due to the different size of Gd^{3+} and Yb^{3+} ions, the diffraction peaks are slightly shifted when the concentration of Yb^{3+} is increased.

First of all, it is clear from the emission of the Er^{3+}/Yb^{3+} core-only nanoparticles (from Figure 6) that an increase of Yb^{3+} concentration pushes the overall observed emission of the Er^{3+} ions toward the red, as expected.[35] Then, the addition of the different layers, first the Tm^{3+}/Yb^{3+}-doped one and then the undoped $NaGdF_4$ one, adds a blue contribution to the spectra that brings the emission color closer to the white, although depending on the starting Yb^{3+} concentration of the core, the actual emission color ranges from cyan (for [Yb^{3+}] = 20 mol %) to pink (for [Yb^{3+}] = 90 mol %). In any case, when the positions of the dopants change and Tm^{3+}/Yb^{3+} ions are moved to the core, the emission color moves to the blue since the Tm^{3+} contribution is now stronger than the $NaGdF_4$:Er^{3+}, Yb^{3+} shell.

Therefore, it is clear that using a core/shell strategy it is possible to exploit independently the luminescent possibilities of the Er^{3+}/Yb^{3+} and Tm^{3+}/Yb^{3+} ion pairs while minimizing the Er^{3+}−Tm^{3+} cross-talk. This opens the path to a broad range of emission-tuning possibilities. In terms of color and for the dopants and concentrations chosen in this work, this range goes from green to red and to blue, including all the intermediate hues and always using 975 nm excitation.

In conclusion, $NaGdF_4$:Tm^{3+}, Yb^{3+} and $NaGdF_4$:Er^{3+}, Yb^{3+} ultrasmall homogeneous upconverting nanoparticles with doped and undoped shells have been synthesized following a microwave-based thermolysis procedure. The formation of core/shell and core/shell/shell nanoarchitectures using this technique allows the doping with both pairs of dopants, spatially separated in the nanoparticles. Then, it has been demonstrated that depending on the position of the dopants inside the nanoparticle architecture, the intensity ratios of the different emission bands change, and thus, the overall emission color is different in each case. Exploiting the fact that Er^{3+}−Tm^{3+} cross-talk is minimized in the proposed structure (due to their spatial segregation), and therefore the luminescent properties of the Er^{3+}/Yb^{3+} and Tm^{3+}/Yb^{3+} ion pairs can be exploited separately, it has been shown that it is possible to tune the overall emission color of the luminescence keeping the excitation wavelength constant at 975 nm.

■ ASSOCIATED CONTENT

Supporting Information

Further details on the synthesis, morphology, and optical characterization of every family of nanoparticles used throughout this paper can be found in the Supporting Information. This material is available free of charge via the Internet at http://pubs.acs.org.

■ AUTHOR INFORMATION

Corresponding Authors

*E-mail: ma@emt.inrs.ca.
*E-mail: vetrone@emt.inrs.ca.

Author Contributions

[†]M. Quintanilla and F. Ren contributed equally to this work.

Notes

The authors declare no competing financial interest.

■ ACKNOWLEDGMENTS

Prof. F. Vetrone is grateful for financial support from the Natural Sciences and Engineering Research Council (NSERC) of Canada, the Canadian Institute for Photonic Innovations (CIPI), and the Fonds de Recherche du Québec − Nature et Technologies (FRQNT) for supporting his research. D.M. is grateful for financial support from NSERC and FRQNT for supporting her research. M.Q. would like to thank Fundación Ramón Areces for financially supporting her through their granting program for Life and Matter Sciences. F.R. would like to thank FQRNT for his Merit Scholarship for Foreign Students.

■ REFERENCES

(1) Mader, H. S.; Kele, P.; Saleh, S. M.; Wolfbeis, O. S. Upconverting luminescent nanoparticles for use in bioconjugation and bioimaging. *Curr. Opin. Chem. Biol.* **2010**, *14*, 582−596.

(2) Zhou, J.; Liu, Z.; Li, F. Upconversion nanophosphors for small-animal imaging. *Chem. Soc. Rev.* **2012**, *41*, 1323−1349.

(3) Wang, C.; Cheng, L.; Liu, Z. Upconversion nanoparticles for potential cancer threanostics. *Ther. Delivery* **2011**, *2*, 1235−1239.

(4) Wang, F.; Banerjee, D.; Liu, Y.; Chen, X.; Liu, X. Upconversion nanoparticles in biological labeling, imaging and therapy. *Analyst* **2010**, *135*, 1839−1854.

(5) Dong, B.; Cao, B.; He, Y.; Liu, Z.; Li, Z.; Feng, Z. Temperature sensing and in vivo imaging by molybdenum sensitized visible upconversion luminescence of rare-earth oxides. *Adv. Mater.* **2012**, *24*, 1987−1993.

(6) Vetrone, F.; Naccache, R.; Zamarron, A.; Juarranz de la Fuente, A.; Sanz-Rodriguez, F.; Maestro, L. M.; Rodriguez, E. M.; Jaque, D.; Sole, J. G.; Capobianco, J. A. Temperature sensing using fluorescent nanothermometers. *ACS Nano* **2010**, *4*, 3245−3258.

(7) Wang, C.; Cheng, L.; Liu, Z. Drug delivery with upconversion nanoparticles for multi-functional targeted cancer cell imaging and therapy. *Biomaterials* **2011**, *32*, 1110−1120.

(8) Ang, L. Y.; Lim, M. E.; Ong, L. C.; Zhang, Y. Applications of upconversion nanoparticles in imaging, detection and therapy. *Nanomed. Nanotechnol. Biol. Med.* **2011**, *6*, 1273−1288.

(9) Zhou, N.; Ni, J.; He, R. Advances of upconversion nanoparticles for molecular imaging. *Nano Biomed. Eng.* **2013**, *5*, 131−139.

(10) Billinton, N.; Knight, A. W. Seeing the wood through the trees: a review of techniques for distinguishing green fluorescent protein from endogenous autofluorescence. *Anal. Biochem.* **2001**, *291*, 175−197.

(11) Monici, M. Cell and tissue autofluorescence research and diagnostic applications. *Biotechnol. Annu. Rev.* **2005**, *11*, 227−256.

(12) Smith, A. M.; Mancini, M. C.; Nie, S. Bioimaging: second window for in vivo imaging. *Nat. Nanotechnol.* **2009**, *4*, 710−711.

(13) Fischer, L. F.; Harms, G. S.; Wolfbeis, O. S. Upconverting nanoparticles for nanoscale thermometry. *Angew. Chem., Int. Ed.* **2011**, *50*, 4546−4551.

(14) Wang, M.; Abbineni, G.; Clevenger, A.; Mao, C.; Xu, S. Upconversion nanoparticles: synthesis, surface modification and biological applications. *Nanomed. Nanotechnol. Biol. Med.* **2011**, *7*, 710−729.

(15) Mendez-Ramos, J.; Acosta-Mora, P.; Ruiz-Morales, J.; Hernandez, T.; Borges, M.; Esparza, P. Turning into the blue: materials for enhancing TiO_2 photocatalysis by up-conversion photonics. *RSC Adv.* **2013**, *3*, 23028−23034.

(16) Park, K.; Lee, S.; Kang, E.; King, K.; Choi, K.; Kwon, I. C. New generation of multifunctional nanoparticles for cancer imaging therapy. *Adv. Funct. Mater.* **2009**, *19*, 1553−1566.

(17) Nie, S.; Xing, Y.; Kim, G. J.; Simons, J. W. Nanotechnology applications in cancer. *Annu. Rev. Biomed. Eng.* **2007**, *9*, 257−288.

(18) Maestro, L. M.; Rodriguez, E. M.; Vetrone, F.; Naccache, R.; Ramirez, H. L.; Jaque, D.; Capobianco, J. A.; Sole, J. G. Nanoparticles for highly efficient multiphoton fluorescence imaging. *Opt. Express* **2010**, *18*, 23544−23553.

(19) Auzel, F. Compteur quantique par transfert d'énergie entre deux ions de terres rares dans un tungstate mixte et dans un verre. *C. R. Acad. Sci. Paris* **1966**, *262*, 1016−1019.

(20) Wang, F.; Liu, X. Recent advances in the chemistry of lanthanide-doped upconversion nanocrystals. *Chem. Soc. Rev.* **2009**, *38*, 976−989.

(21) Hewes, R. A.; Sarver, J. F. Infrared excitation processes for the visible luminescence of Er^{3+}, Ho^{3+}, and Tm^{3+} in Yb^{3+}-sensitized rare-earth trifluorides. *Phys. Rev. B: Condens. Matter* **1969**, *182*, 427−436.

(22) Rapaport, A.; Milliez, J.; Bass, M.; Cassanho, A.; Jenssen, H. Review of the properties of up-conversion phosphors for new emissive displays. *J. Dispersion Technol.* **2006**, *2*, 68−78.

(23) Jiang, C.; Xu, W. B. Theoretical model of Yb^{3+} - Er^{3+} - Tm^{3+} - codoped system for white light generation. *J. Dispersion Technol.* **2009**, *5*, 312−318.

(24) Yeh, D. C.; Petrin, R. R.; Sibley, W. A.; Madigou, V.; Adam, J. L.; Suscavage, M. J. Energy transfer between Er^{3+} and Tm^{3+} ions in barium fluoride-thorium fluoride glass. *Phys. Rev. B: Condens. Matter* **1989**, *23*, 80−90.

(25) Yan, D.; Zhu, J.; Wu, H.; Yang, Z.; Qiu, J.; Song, Z.; Yu, X.; Yang, Y.; Zhou, D.; Yin, Z.; Wang, R. Energy transfer and photoluminescence modification in Yb-Er-Tm triply doped $Y_2Ti_2O_7$ upconversion inverse opal. *J. Mater. Chem.* **2012**, *22*, 18558−18563.

(26) Xiao, Z.; Serna, R.; Afonso, C. N.; Cheng, G.; Vickridge, I. Improving the photoluminescence response of Er-Tm: Al_2O_3 films by Yb codoping. *J. Lumin.* **2007**, *122−123*, 32−35.

(27) Mayer, F.; Peters, J. A.; Djanashvili, K. Microwave-assisted seeded growth of lanthanide-based nanoparticles for imaging and therapy. *Chem.—Eur. J.* **2012**, *18*, 8004−8007.

(28) Wang, H.-Q.; Nann, T. Monodisperse upconverting nanocrystals by microwave-assisted synthesis. *ACS Nano* **2009**, *3*, 3804−3808.

(29) Baghbanzadeh, M.; Carbone, L.; Cozzoli, P. D.; Kappe, C. O. Microwave-assisted synthesis of colloidal inorganic nanocrystals. *Angew. Chem.* **2011**, *50*, 11312−11359.

(30) Rodriguez-Liviano, S.; Aparicio, F. J.; Rojas, T. C.; Hungria, A. B.; Chinchilla, L. E.; Ocaña, M. Microwave-assisted synthesis and luminescence of mesoporous RE-doped YPO4 (RE = Eu, Ce, Tb, and Ce + Tb) nanophosphors with lenticular shape. *Cryst. Growth Des.* **2012**, *12*, 635−645.

(31) Niu, N.; He, F.; Gai, S.; Li, C.; Zhang, X.; Huang, S.; Yang, P. Rapid microwave reflux process for the synthesis of pure hexagonal $NaYF_4$:Yb^{3+}, Ln^{3+}, Bi^{3+} (Ln^{3+} = Er^{3+}, Tm^{3+}, Ho^{3+}) and its enhanced UC luminescence. *J. Mater. Chem.* **2012**, *22*, 21623.

(32) Boyer, J.-C.; Vetrone, F.; Cuccia, L. A.; Capobianco, J. A. Synthesis of colloidal upconverting $NaYF_4$ nanocrystals doped with Er^{3+}, Yb^{3+} and Tm^{3+}, Yb^{3+} via thermal decomposition of lanthanide trifluoroacetate precursors. *J. Am. Chem. Soc.* **2006**, *128*, 7444−7445.

(33) Quintanilla, M.; Nuñez, N.; Cantelar, E.; Ocaña, M.; Cusso, F. Tuning from blue to magenta the up-converted emissions of YF_3:Tm^{3+}/Yb^{3+} nanocrystals. *Nanoscale* **2011**, *3*, 1046−1052.

(34) Heer, S.; Kömpe, K.; Güdel, H.-U.; Haase, M. Highly efficient multicolour upconversion emission in transparent colloids of lanthanide-doped $NaYF_4$ nanocrystals. *Adv. Mater. 16*, 2102−2105.

(35) Wang, F.; Liu, X. Upconversion multicolor fine-tuning: visible to near-infrared emission from lanthanide-doped $NaYF_4$ nanoparticles. *J. Am. Chem. Soc.* **2008**, *130*, 5642−5643.

(36) Chen, G. Y.; Ohulchanskyy, T. Y.; Liu, S.; Law, W. C.; Wu, F.; Swihart, M. T.; Agren, H.; Prasad, P. N. Core/Shell $NaGdF_4$:Nd^{3+}/$NaGdF_4$ Nanocrystals with Efficient Near-Infrared to Near-Infrared Downconversion Photoluminescence for Bioimaging Applications. *ACS Nano* **2012**, *6*, 2969−2977.

(37) Boyer, J.-C.; van Veggel, F. C. J. M. Absolute quantum yield measurements of colloidal $NaYF_4$:Er^{3+}/Yb^{3+} upconverting nanoparticles. *Nanoscale* **2010**, *2*, 1417−1419.
(38) Shen, J.; Chen, G.; Ohulchanskyy, T. Y.; Kesseli, S. J.; Buchholz, S.; Li, Z.; Prasad, P. N.; Han, G. Tunable near infrared to ultraviolet upconversion luminescence enhancement in (alpha-$NaYF_4$:Yb,Tm)/CaF_2 core/shell nanoparticles for in situ real-time recorded biocompatible photoactivation. *Small* **2013**, *9*, 3213−3217.
(39) Dexter, D. L.; Miyakawa, T. Cooperative and stepwise excitation of luminescence: trivalent rare-earth ions in Yb^{3+}-sensitized crystals. *Phys. Rev. B: Condens. Matter* **1970**, *1*, 70−80.
(40) Auzel, F. Upconversion and anti-stokes processes with *f* and *d* ions in solids. *Chem. Rev.* **2004**, *104*, 139−173.
(41) De, G.; Qin, W. P.; Zhang, J. S.; Zhang, J. S.; Wang, Y.; Cao, C. Y.; Cui, Y. Infrared-to-ultraviolet up-conversion luminescence of YF_3:Yb^{3+},Tm^{3+} microsheets. *J. Lumin.* **2007**, *122*−*123*, 128−130.
(42) Wang, G. F.; Qin, W. P.; Wang, L. L.; Wei, G. D.; Zhu, P.; Kim, R. J. Intense ultraviolet upconversion luminescence from hexagonal $NaYF_4$:Yb^{3+}/Tm^{3+} microcrystals. *Opt. Express* **2008**, *16*, 11907−11914.
(43) Wang, F.; Wang, J.; Liu, X. Direct evidence of a surface quenching effect on size-dependent luminescence of upconversion nanoparticles. *Angew. Chem., Int. Ed.* **2010**, *49*, 7456−7460.
(44) Nuñez, N.; Quintanilla, M.; Cantelar, E.; Cusso, F.; Ocaña, M. Uniform YF_3:Yb,Er up-conversion nanophosphors of various morphologies synthesized in polyol media through an ionic liquid. *J. Nanopart. Res.* **2010**, *12*, 2553−2565.
(45) Vetrone, F.; Naccache, R.; Mahalingam, V.; Morgan, C. G.; Capobianco, J. A. The active-core/active-shell approach: a strategy to enhance the upconversion luminescence in lanthanide-doped nanoparticles. *Adv. Funct. Mater.* **2009**, *19*, 2924−2929.
(46) Qian, H.-S.; Zhang, Y. Synthesis of hexagonal-phase core-shell $NaYF_4$ nanocrystals with tunable upconversion fluorescence. *Langmuir* **2008**, *24*, 12123−12125.
(47) Wang, F.; Deng, R.; Wang, J.; Wang, Q.; Han, Y.; Zhu, H.; Chen, X.; Liu, X. Tuning upconversion through energy migration in core-shell nanoparticles. *Nat. Mater.* **2011**, *10*, 968−973.
(48) Abel, K. A.; Boyer, J. C.; van Veggel, F. C. J. M. Hard proof of the $NaYF_4$/$NaGdF_4$ nanocrystal core/shell structure. *J. Am. Chem. Soc.* **2009**, *131*, 14644−14645.
(49) Passuello, T.; Piccinelli, F.; Pedroni, M.; Bettinelli, M.; Mangiarini, F.; Naccache, R.; Vetrone, F.; Capobianco, J. A.; Speghini, A. White light upconversion of nanocrystalline Er/Tm/Yb doped tetragonal $Gd_4O_3F_6$. *Opt. Mater.* **2011**, *33*, 643−646.
(50) Etchart, I.; Berard, M.; Laroche, M.; Huignard, A.; Hernandez, I.; Gillin, W. P.; Curry, R. J.; Cheetham, A. K. Efficient white light emission by upconversion in Yb^{3+}-, Er^{3+}- and Tm^{3+}-doped Y_2BaZnO_5. *Chem. Commun.* **2011**, *47*, 6263−6265.
(51) Huang, L.; Wang, L.; Xue, X.; Zhao, D.; Qin, G.; Qin, W. Enhanced red upconversion luminescence in Er-Tm codoped $NaYF_4$ phosphor. *J. Nanosci. Nanotechnol.* **2011**, *11*, 9498−9501.
(52) Zhang, Y.; Hao, J. Color-tunable upconversion luminescence of Yb^{3+}, Er^{3+}, and Tm^{3+} tri-doped ferroelectric $BaTiO_3$ materials. *J. Appl. Phys.* **2013**, *113*, 184112.
(53) Chen, D.; Wang, Y. S.; Zheng, K.; Guo, T. L.; Yu, Y. L. Bright upconversion white light emission in transparent glass ceramic embedding Tm^{3+}/Er^{3+}/Yb^{3+}:β-YF_3 nanocrystals. *Appl. Phys. Lett.* **2007**, *91*, 251903.